



Quantum interferometric spectroscopy of a biexciton

Hiroya Seki ¹, Kensuke Miyajima ², and Ryosuke Shimizu¹

¹*Department of Engineering Science, Graduate School of Informatics and Engineering, The University of Electro-Communications, 1-5-1 Chofugaoka, Chofu, Tokyo 182-8585, Japan*

²*Department of Applied Physics, Graduate School of Science, Tokyo University of Science, 6-3-1 Niijuku, Katsushika-ku, Tokyo 125-8585, Japan*



(Received 1 November 2021; accepted 28 November 2022; published 22 December 2022)

Fourier transform spectroscopy with classical interferometry corresponds to the measurement of a single-photon intensity spectrum from the viewpoint of the particle nature of light. In contrast, the Fourier transform of two-photon quantum interference patterns provides the intensity spectrum of the two photons as a function of the sum- or difference frequency of the constituent photons. This unique feature of quantum interferometric spectroscopy offers a different type of spectral information from the classical measurement and may prove useful for nonlinear spectroscopy with two-photon emission. Here, we report the experimental demonstration of two-photon quantum interference of biphotons emitted via biexcitons in the semiconductor CuCl. Besides applying Fourier transform to quantum interference patterns, we reconstruct the intensity spectrum of the biexciton luminescence in the two-photon sum- or difference frequency. We discuss the connection between the reconstructed spectra and exciton states in CuCl as well as the capability of quantum interferometry in solid-state spectroscopy.

DOI: [10.1103/PhysRevA.106.063716](https://doi.org/10.1103/PhysRevA.106.063716)

I. INTRODUCTION

Interference of the quantum field of multiple photons involves versatile phenomena in quantum science and technology. The first experimental demonstration, known as the Hong-Ou-Mandel (HOM) effect, was reported in 1987 [1]. Since then, this phenomenon has been widely used, ranging from the testing of the fundamental concepts of quantum mechanics [2–6] to quantum communications [7,8] or photonic quantum logic gate [9,10]. Another type of quantum interference is that the interferometric fringe shows the sum of the frequencies of the constituent photons, which is known as NOON-state interference [11]. This type of quantum interference has evolved through high-precision phase measurement [11–13] or high-resolution imaging [14]. These two types of quantum interference have been studied independently, but it is possible to explain all the phenomena by calculating the higher-order correlation function.

We recently proposed a connection between HOM- or NOON-state two-photon interference fringes and the spectral information, and this connection is underpinned by the Wiener-Khinchin formalism [15]. While the conventional Wiener-Khinchin theorem [16,17] is dedicated to the first-order correlation function, we termed the relation with a second-order correlation function for the two-photon quantum interference phenomena an extended Wiener-Khinchin theorem (e-WKT) [15]. This formalism provides a comprehensive and intuitive understanding of two-photon interference; the Fourier transform of the HOM- (NOON) fringe gives the difference- (sum-) frequency spectrum of the two constituent photons. Furthermore, the formalism could enable us to accelerate the exploitation of spectroscopic measurements with two-photon interference. Hereafter, we refer to the

interferometric measurement based on e-WKT as quantum Fourier transform spectroscopy (QFTS).

In our previous experiment, we demonstrated a proof-of-principle experiment of the e-WKT utilizing photon pairs from spontaneous parametric down-conversion (SPDC) in a nonlinear crystal. The physical process of SPDC is relatively simple and easy to handle; the resultant spectral characteristics from the e-WKT can be understood by the properties of the pump-pulse spectrum and the dispersion relation of the nonlinear crystal [18]. On the other hand, a feasibility study with a complex physical system, such as condensed matter, is desirable for the further development of QFTS as a form of practical spectroscopy. To this end, here we present the quantum Fourier transform spectroscopy of a biexciton in a single crystal of the semiconductor CuCl.

II. METHODS AND RESULTS

A. Biphoton emission via biexciton in CuCl

CuCl single crystal provides a simple exciton band structure, and thus its exciton properties have been intensively investigated since the early stage of solid-state spectroscopy [19,20]. Furthermore, CuCl is known as the material used for the first entangled-state generation from a semiconductor [21], while many works using semiconductor quantum dots have been reported [22–25]. Unlike entangled-photon generation in semiconductor quantum dots, entangled-state generation in CuCl is obtained via resonant hyperparametric scattering (RHPS) accompanied by the phase-matching condition in the transition between biexciton and exciton-polariton bands: a biexciton is created by resonant two-photon excitation and then coherently decays into two exciton-polaritons. These

polaritons propagate inside the crystal in the direction determined by the phase-matching condition and subsequently convert into photons at the crystal surface. In what follows, we refer to a photon from a higher- (lower-) energy polariton as a HEP (LEP) photon. The presence of the phase-matching condition makes it easy to collect photon pairs at certain emission angles, similar to photon-pair generation with nonlinear crystals [26]. Such well-characterized excitonic properties and photon-pair generation in CuCl can offer a superior environment for the demonstration of QFTS as a step toward solid-state spectroscopy with quantum interferometry.

CuCl crystals were grown by a vapor-phase transport method. CuCl powders (Sigma-Aldrich; purity of 99.9995%) were put on a quartz boat, which was then inserted in a quartz tube. The quartz tube was then filled with Ar gas of 0.3 atm, then sealed. Using an electric furnace, the CuCl powders were heated at 430 °C for approximately 14 days, during which CuCl single crystals grew as platelets on the tube's internal wall. The thickness of the CuCl platelets was approximately several tens of micrometers.

The experimental setup for the generation and collection of photon pairs is depicted in Fig. 1(a). CuCl was pumped by a frequency-doubled mode-locked Ti:sapphire laser with a repetition rate of 76 MHz. The center wavelength of the second-harmonic light was tuned at 389 nm with a bandwidth of 0.1 nm for the resonant two-photon excitation of the biexciton. The sample was kept at a temperature of 3.9 K, and the pump beam irradiated CuCl with normal incidence. Then the photon pairs, symmetrically emitted at an angle of 20° to the propagation direction of the pump beam, were collected into polarization-maintaining fibers (PMFs). Figure 1(b) shows the spectra of the photons scattered into the upper optical path in Fig. 1(a) with an average pump beam power of 4.0 μW, taken by a charge-coupled device camera with a grating spectrometer. The peaks indicated by HEP and LEP are the spectra of photon pairs, and the Rayleigh scattered light of the pump beam appears between the HEP and LEP spectra. The other peaks, labeled M_T , M_L , and HEP', also originated from the biexciton luminescence but do not form a two-photon state. Thus, in this work we focus only on the spectral peaks of HEP and LEP. A previous report demonstrated the generation of entanglement in the polarization degree of freedom [21], but the biphotons from the biexciton in CuCl are expected to have entanglement in the frequency degree of freedom simultaneously. Therefore, the two-photon state observed in paths 1 and 2 might be in hyperentanglement as follows: $(|H\rangle_1|H\rangle_2 + |V\rangle_1|V\rangle_2) \otimes (|\omega_{\text{HEP}}\rangle_1|\omega_{\text{LEP}}\rangle_2 + |\omega_{\text{LEP}}\rangle_1|\omega_{\text{HEP}}\rangle_2)$, where H , V , ω_{HEP} , and ω_{LEP} represent the states for the horizontal, vertical, and angular frequencies of HEP and LEP photons (indicated by $i = 1, 2$), respectively. Such inherent characteristics of the hyperentangled state via RHPS will be discussed elsewhere. In the present study, since only the frequency entanglement is needed to observe the two-photon quantum interference, we placed polarizing beam splitters (PBSs) before the PMFs.

B. Two-photon quantum interferometer

For the HOM- and NOON-state interferometry, we constructed a polarization mode, not a standard-path mode,

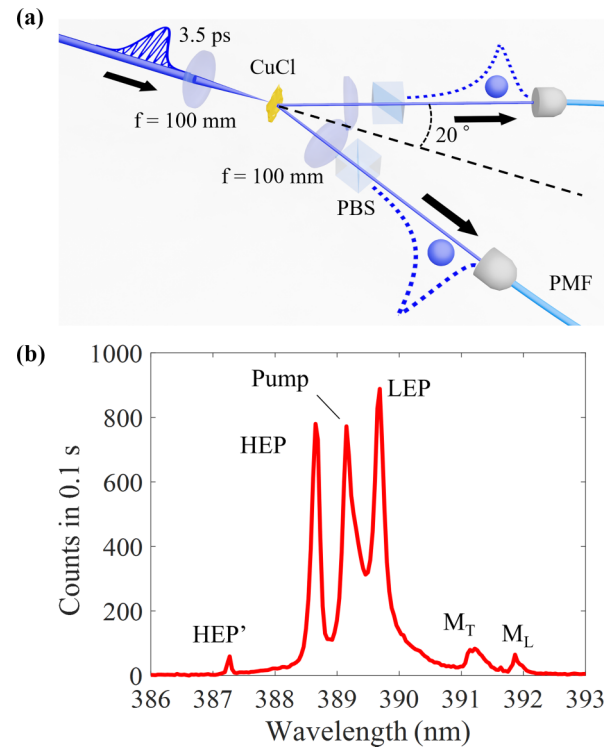


FIG. 1. Biphoton generation in CuCl single crystal. (a) Schematic of the generation of photon pairs and their collection into polarization-maintaining fibers (PMFs). Polarizing beam splitters (PBSs) work not only to select a frequency-entangled state but also to reduce the Rayleigh scattered pump beam. (b) Emission spectrum of the CuCl at 3.9 K with two-photon resonant excitation. The peaks of HEP and LEP are the photon-pair spectra via RHPS. The residual pump beam (pump) is observed between the HEP and LEP spectra. The two peaks of M_T and M_L in the lower-energy side are the biexciton luminescences leaving the transverse and longitudinal excitons, respectively. HEP' also originates from RHPS but does not form a two-photon state.

Mach-Zehnder interferometer (MZI), as shown in Fig. 2(a). The use of polarization modes provides a versatile interferometer setup just by rotating the half-wave plates (HWPs). Here, we oriented the axes of PMFs so that the polarization of the two photons was orthogonal to each other at the input side of the interferometer. In addition, we adjusted the temporal delay between the two photons from each fiber to be zero. After the spatial and temporal modes of the two photons were combined by a polarizing beam splitter (PBS1), photon pairs were fed into the polarization-mode MZI. Outputted photon pairs from the interferometer were coupled into multimode fibers (MMFs) after the spatial mode was divided by a polarizing beam splitter (PBS3). We then performed coincidence measurements with two single-photon avalanche diodes (SPADs) and a time-interval analyzer.

The quarter-wave plates (QWP1 and 2) inside the interferometer were fixed at the optical axes of 22.5° to the horizontal axis. When all the optical axes of the HWPs were set to 0°, no interferometric effects were observed. In order to work as a HOM interferometer, we set HWP2 to 22.5° while HWP1 is kept at 0°, as shown in Fig. 2(b). We controlled the relative

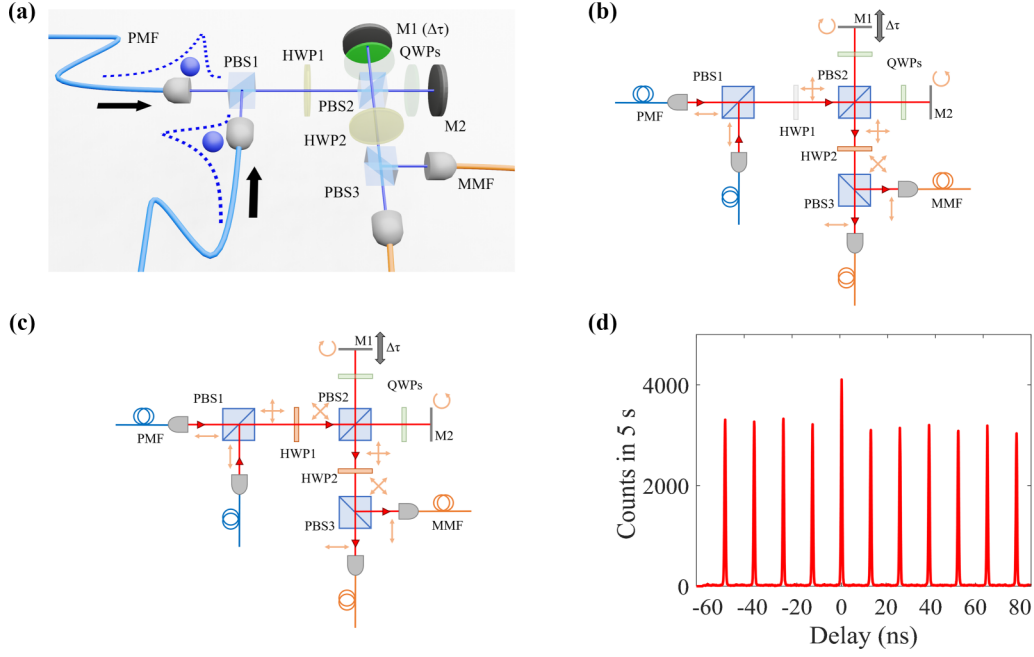


FIG. 2. Two-photon quantum interferometer. (a) Schematic of the polarization-mode Mach-Zehnder interferometer. The time delay $\Delta\tau$ for the HOM- and the NOON-state interference were controlled by scanning the position of the mirror M1. (b) Simple diagram of polarization in each optical path in HOM interference. (c) Simple diagram of polarization in each optical path in NOON-state interference. (d) Time-correlation histogram of photon pairs through the interferometer when setting the half-wave plates (HWP1 and HWP2) to 0° . The central peak at the delay time of zero contains photon-pair signals.

delay ($\Delta\tau$) between the two photons at PBS3 by scanning the mirror (M1) position. Photons reflected by M1 and M2 interfered in the polarization mode at PBS3, and then the HOM interference effect was observed. On the other hand, the NOON-state interferometer in Fig. 2(c) was realized by setting both HWP1 and HWP2 to 22.5° . Setting HWP1 to 22.5° induces the HOM interference effect at PBS2. Thus, the two photons were outputted to either interferometer arm, indicating the NOON state was created with the polarization mode. Setting HWP2 to 22.5° , we could observe the NOON-state interference at PBS3 by scanning $\Delta\tau$. Here, we emphasize that no spectral filter was used in any of the measurements because we intended to demonstrate the extraction of spectral information only by the QFTS. Thus, all the spectral components, as shown in Fig. 2(b), contributed to the photon-counting measurements.

Figure 2(b) shows the histogram of the time-interval analysis of the photon-counting signals from the two SPADs. We saw slightly larger peak counts at the delay time of 0 ns and estimated the accidental coincidence counts in the peak at the zero-delay position from the counting values in the side peaks. Then, subtracting the accidental counts as background, we recorded the coincidence counts caused by the photon pairs.

The spectroscopic capability of the coincidence counting measurement is worth discussing. The coincidence measurement works to extract only the photon-pair spectral components. In our case, we recorded the coincidence counting rate of ~ 1600 counts/s against the single-photon counting rate of $\sim 650\,000$ counts/s, meaning a signal-to-noise ratio of 0.25%. Even under such conditions, we could select the spectra of the HEP and LEP apart from the other biexciton luminescences and the Rayleigh scattered light of the

pump beam, without any spectral filters, by only coincidence measurements. The second-order correlation measurement provides a powerful tool not only for quantum information technologies but also for spectroscopic quantum measurements.

C. Extended Wiener-Khinchin theorem

The two-photon detection probabilities for the NOON-state interference P_2^+ and for the HOM interference P_2^- are given by the following form:

$$P_2^\pm(\tau) = \frac{1}{2} \left\{ 1 \pm \text{Re} \left[\int_{-\infty}^{\infty} \int_{-\infty}^{\infty} d\omega_1 d\omega_2 |f_2(\omega_1, \omega_2)|^2 \times e^{-i(\omega_1 \pm \omega_2)\Delta\tau} \right] \right\}, \quad (1)$$

where $f_2(\omega_1, \omega_2)$ is the two-photon spectral probability amplitude for the photons with angular frequencies ω_1 and ω_2 . The symmetry condition, $f_2(\omega_1, \omega_2) = f_2(\omega_2, \omega_1)$, is needed for this expression, but we can expect that the biphotons from CuCl would be satisfied. Here, we introduce the sum-frequency spectrum F_2^+ and the difference-frequency spectrum F_2^- as $F_2^\pm(\omega_\pm) \equiv \int_{-\infty}^{\infty} d\omega_\mp |f_2(\omega_\pm, \omega_\mp)|^2$, where $\omega_\pm = \omega_1 \pm \omega_2$. Then, the two-photon detection probabilities are rewritten as

$$P_2^\pm(\tau) = \frac{1}{2} \left\{ 1 \pm \text{Re} \left[\int_{-\infty}^{\infty} d\omega_\pm F_2^\pm(\omega_\pm) e^{-i\omega_\pm \Delta\tau} \right] \right\}. \quad (2)$$

This equation describes that the Fourier transform of the sum- or difference-frequency spectrum provides the two-photon quantum interference pattern. Moreover, we can define

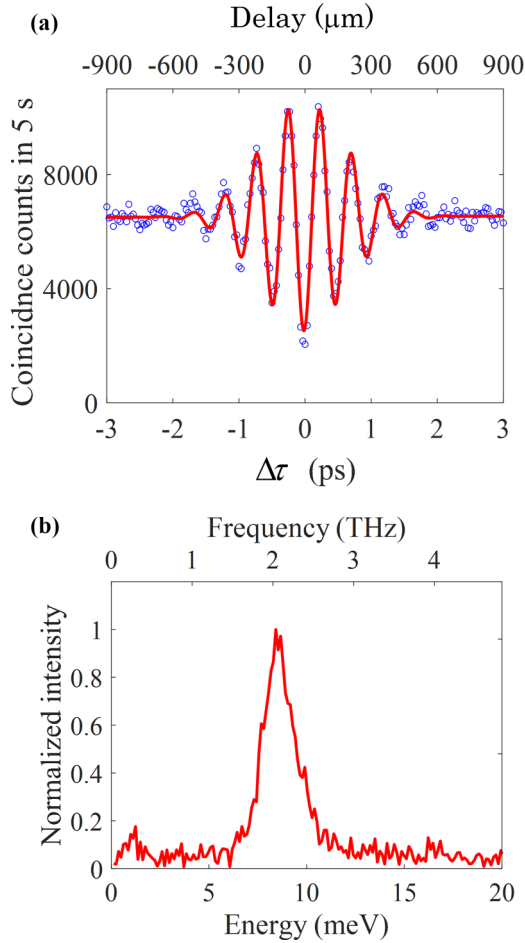


FIG. 3. Fourier transform spectroscopy with HOM interference. (a) Two-photon coincidence counts as a function of the delay of $\Delta\tau$ when HWP1 and HWP2 are set to 0° and 22.5° in Fig. 2(a), respectively. This setup provides the HOM interference pattern. Open circles are the measured data, and the solid curve is obtained from the fitting. (b) Difference-frequency spectrum of biphotons by making the fast Fourier transform of the HOM patterns in (a).

the second-order correlation function as the Fourier transform of the F_2^\pm :

$$G_2^\pm(\tau) \equiv \int_{-\infty}^{\infty} d\omega_\pm F_2^\pm(\omega_\pm) e^{-i\omega_\pm \Delta\tau}. \quad (3)$$

For the inverse Fourier transform, we obtain

$$F_2^\pm(\omega_\pm) = \frac{1}{2\pi} \int_{-\infty}^{\infty} d\tau G_2^\pm(\tau) e^{i\omega_\pm \Delta\tau}. \quad (4)$$

These Fourier transform relations between the F_2^\pm and the G_2^\pm are the extended Wiener-Khinchin theorem, which underpins the quantum Fourier transform spectroscopy presented in this paper.

D. Fourier transform spectroscopy by quantum interferometry

We start by discussing the HOM interference experiment in advance of the two-photon NOON-state interference because the NOON-state interference is performed as the extension of the HOM interference. Figure 3(a) presents the resultant HOM

interference fringe pattern with a visibility of 61% in our experiment. Here, we emphasize that this is the experimental observation of the HOM interference of biphotons generated from biexciton luminescence, even though HOM experiments with single photons from semiconductor quantum dots were conducted to test the indistinguishability [27]. The visibility value is somewhat lower than that by photon pairs from SPDC but high enough to perform Fourier transform spectroscopy. According to the e-WKT, we applied the fast Fourier transform (FFT) to our data and then obtained the difference-frequency spectrum of biphotons from the biexciton, as shown in Fig. 3(b). The peak position of the spectrum, 8.6 meV, is associated with the oscillation frequency of the HOM that originated from the frequency difference between the HEP and LEP photons. In practice, the spectral peak separation between the HEP and LEP in Fig. 1(b) is 8.3 meV and agrees nicely with the Fourier-transformed spectrum. These peak positions can be estimated by the phase-matching condition for RHPS [21], implying that the dispersion relation of the exciton-polariton would be dominant for the characteristics of the difference-frequency spectrum. Besides, the coherence time in the HOM is relevant to the spectral width of the difference-frequency spectrum. This spectral width value of 1.93 meV is mostly twice that by the HEP or LEP in Fig. 1(b) because the FFT spectrum is provided as a function of the difference frequency between the HEP and LEP photons.

Following the HOM experiment, we carried out the NOON-state interference experiment. Figure 4(a) represents the fringe pattern around the zero-delay position of the interferometer. Fitting the pattern with a sinusoidal function, we estimated an oscillation period of 195 ± 39 nm with a visibility of 82%. From the viewpoint of the e-WKT, this period means the sum of the frequencies of the constituent photons. Eventually, we estimated the sum energy of the two photons as 6.37 ± 1.57 eV from the period of NOON-state interference pattern. This sum-energy value should correspond to the biexciton energy because of the phase-matching condition in the RHPS process. The energy level of the biexciton in CuCl was precisely investigated and identified to be 6.37 eV in the earlier experiment with four-wave mixing nonlinear spectroscopy [28]. Note that Fourier transform spectroscopy is not suitable for estimating precise energy levels in a short-wavelength range, but enables to provide us a better estimation of spectral shapes regardless of the wavelength range. For further spectral analysis, we carried out a long-range interferometric measurement to observe the envelope shape of the fringe pattern. In this measurement, we took coincidence counts for 5 s by scanning every $5 \mu\text{m}$. Ideally, the scanning step should be a much shorter value than the oscillation period, but we had technical difficulties in retaining the stability of the NOON-state interferometer during the long measurement time. Thus, we observed the envelope shape separately from the oscillation period, assuming that only the single sum-frequency oscillation would contribute to the interference pattern. Figure 4(b) shows the observed pattern with coarse scanning for the long-range measurement. In SPDC experiments, it is well known that the coherence time that appeared in the NOON-state interference is relevant to that of the pump pulse. However, the coherence time of the interference in Fig. 4(b) is approximately 17 ps, which

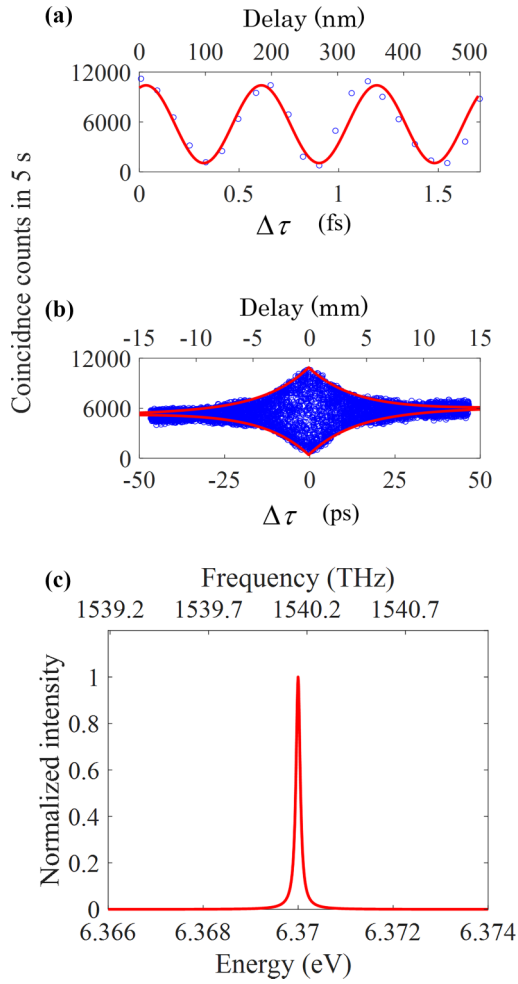


FIG. 4. Fourier transform spectroscopy with NOON-state interference. Two-photon coincidence counts as a function of the delay of $\Delta\tau$ when all the HWPs are set to 22.5° in Fig. 2(a), providing the NOON-state interference pattern around the zero-delay position (a) and in the long-range scanning (b). The solid curve in (a) is the fitting for the interferometric oscillation and that in (b) for the envelope shape. (c) Sum-frequency spectrum of biphotons obtained from the Fourier transform of the reproduced interference pattern from the fitting curves.

is much longer than the pump-pulse duration of 3.4 ps. In a previous experiment on the biexciton in CuCl, the dephasing time of the biexciton measured at 4 K was reported as 16 ps [29] by nonlinear spectroscopy of four-wave mixing. Since the dephasing times of the biexciton in CuCl varied from 16 to 50 [29,30] ps from sample to sample, in the previous experiments, the coherence time observed in the NOON-state interferometry could be considered to reflect the dephasing time of the biexciton.

For the Fourier transform spectroscopy, we assume the following function in order to reproduce the interference pattern: $I(\tau) = e^{-\gamma|\tau|}(1 + V \cos \omega\tau)$ where I , γ , V , and ω are the normalized counting rate, decay rate, visibility, and oscillation frequency, respectively. We estimated the oscillation frequency ω and the visibility V from the fine scanning data around the zero-delay position in Fig. 4(a). On the other hand, the decay rate γ was determined by fitting the envelope

shape in Fig. 4(b). The exponentially decaying function was used in the previous time-resolved measurements of biexciton luminescence [30] and well fitted our observed data indeed. Then, applying the Fourier transform to the reproduced NOON-state interference pattern, we estimated the sum-frequency spectrum, as shown in Fig. 4(c). As discussed above, the center frequency and spectral shape would be purely reflected in the biexciton properties. Additionally, the spectral width of 0.11 meV is much narrower than that of the HEP or LEP spectrum, indicating that it is hard to observe the sum-frequency spectrum by classical spectroscopic measurements. Therefore, we could say that Fourier transform spectroscopy with NOON-state interferometry allows us to measure the biexciton spectrum reflecting the intraband relaxation, thereby distinguishing it from the spectrum determined by the interband transition between the biexciton and the exciton-polariton.

III. DISCUSSION

Conventionally, the single-photon emission caused by the transition from a biexciton state to an intermediate state was previously measured to elucidate biexciton characteristics [29–32]; in our case, the exciton-polariton describes the intermediate state. The characteristics of a single photon, however, are affected by not only the biexciton state but also the intermediate state. Thus, single-photon spectral measurement cannot observe a pure spectrum reflecting the intraband relaxation of a biexciton. On the other hand, as demonstrated in this paper, two-photon spectral measurement allows the measurement of the biexciton spectrum separated from the influence on the intermediate state. This unique feature of QFTS, based on the measurement axes of the sum- or difference frequencies, has great potential for two-photon nonlinear spectroscopy at the single-photon level.

It should be noted that two-photon quantum interferometry requires a symmetric state for interchanging the constituent photons in any degree of freedom. Since biphotons from the biexciton in CuCl naturally satisfy the symmetry condition, we can successfully demonstrate biexciton spectroscopy with QFTS. Symmetry conditions can also be found in photon-pair generation with polarization entanglement. Thus, QFTS could be applicable to the wide variety of materials that can create polarization-entangled photon pairs, such as quantum dots [33], single molecules [34], and proteins [35]. In addition, even if photon pairs do not satisfy the symmetry condition, we might overcome the limitation by creating a superposition state of the two-photon state. Indeed, the symmetry condition can be realized by placing a material inside an interferometer in some quantum optical experiments with nonlinear crystals [36]. This would mitigate the exchange-symmetry condition for QFTS. Our next challenge will be to carry out QFTS for two-photon emission without the symmetry condition in order to establish its versatility.

Additionally, the presence of the phase-matching condition in the RHPS process of CuCl makes it easy to collect photon-pair emissions into optical fibers. However, two-photon emission without any phase-matching condition would often be observed in solid-state spectroscopy, and then the two-photons are randomly emitted in any directions due to

the absence of momentum correlation between the photons. Thus, the development of a means to collect two photons in a wide solid angle would also be crucial for applying QFTS to investigate various condensed matters.

IV. CONCLUSIONS

We demonstrated Fourier transform spectroscopy with quantum interferometry for biphotons produced via the CuCl biexciton. First, we discussed the applicability of two-photon counting measurement to spectroscopy. Consequently, we showed that the second-order correlation measurement could work well as it extracts only the spectral component of the photon pair in a high signal-to-noise ratio and has great potential for the spectroscopy of condensed-matter systems. Secondly, we demonstrated that the two-photon quantum interference provides two types of interferometric waveforms: one gives the fringe with the difference frequency and the other that with the sum frequency of the constituent photons. Another type of QFTS with frequency-entangled photons has been reported, and it is the method to estimate the absorption spectra from a two-photon quantum interference pattern [37,38]. By contrast, the ability to evaluate the sum-

or difference-frequency spectrum by two-photon interference suggests the potential to be applied to fundamental research on nonlinear luminescence. In the case of biexciton luminescence, the Fourier-transformed difference-frequency spectrum can be characterized by the phase-matching condition associated with the dispersion properties of the exciton-polariton. In contrast, the QFTS with the two-photon sum frequency allows us to unveil the spectrum that purely reflects the intraband relaxation of the biexciton. Generally, two-photon emission exhibits an intricate spectrum because of the contributions of multiple quantum states. However, QFTS allows us to observe the two-photon spectrum as a function of the sum- or difference frequency, making it simple to study a composite quantum system, such as a biexciton, as decomposed into each associated state. These remarkable features of QFTS constitute a tool to investigate nonlinear light-matter interactions with two-photon emission.

ACKNOWLEDGMENTS

This work was supported by MEXT Quantum Leap Flagship Program (MEXT Q-LEAP) Grant No. JPMXS0118069242.

-
- [1] C. K. Hong, Z. Y. Ou, and L. Mandel, Measurement of Subpicosecond Time Intervals between Two Photons by Interference, *Phys. Rev. Lett.* **59**, 2044 (1987).
 - [2] D. Bouwmeester, J.-W. Pan, K. Mattle, M. Eibl, H. Weinfurter, and A. Zeilinger, Experimental quantum teleportation, *Nature (London)* **390**, 575 (1997).
 - [3] J. F. Clauser, M. A. Horne, A. Shimony, and R. A. Holt, Proposed Experiment to Test Local Hidden-Valuable Theories, *Phys. Rev. Lett.* **23**, 880 (1969).
 - [4] P. G. Kwiat, A. M. Steinberg, and R. Y. Chiao, Observation of a “quantum eraser”: A revival of coherence in a two-photon interference experiment, *Phys. Rev. A* **45**, 7729 (1992).
 - [5] T. B. Pittman, D. V. Strekalov, A. Migdall, M. H. Rubin, A. V. Sergienko, and Y. H. Shih, Can Two-Photon Interference Be Considered the Interference of Two Photons?, *Phys. Rev. Lett.* **77**, 1917 (1996).
 - [6] A. M. Steinberg, P. G. Kwiat, and R. Y. Chiao, Dispersion Cancellation in a Measurement of the Single-Photon Propagation Velocity in Glass, *Phys. Rev. Lett.* **68**, 2421 (1992).
 - [7] H. Takesue, S. D. Dyer, M. J. Stevens, V. Verma, R. P. Mirin, and S. W. Nam, Quantum teleportation over 100 km of fiber using highly efficient superconducting nanowire single-photon detectors, *Optica* **2**, 832 (2015).
 - [8] V. D’Auria, B. Fedrici, L. A. Ngah, F. Kaiser, L. Labonté, O. Alibart, and S. Tanzilli, A universal, plug-and-play synchronization scheme for practical quantum networks, *NPJ Quantum Inf.* **6**, 21 (2020).
 - [9] P. J. Shadbolt, M. R. Verde, A. Peruzzo, A. Politi, A. Laing, M. Lobino, J. C. F. Matthews, M. G. Thompson, and J. L. O’Brien, Generating, manipulating and measuring entanglement and mixture with a reconfigurable photonic circuit, *Nat. Photonics* **6**, 45 (2012).
 - [10] M. Stobińska, A. Buraczewski, M. Moore, W. R. Clements, J. J. Renema, S. W. Nam, T. Gerrits, A. Lita, W. S. Kolthammer, A. Eckstein, and I. A. Walmsley, Quantum interference enables constant-time quantum information processing, *Sci. Adv.* **5**, eaau9674 (2019).
 - [11] P. Walther, J.-W. Pan, M. Aspelmeyer, R. Ursin, S. Gasparoni, and A. Zeilinger, De Broglie wavelength of a non-local four-photon state, *Nature (London)* **429**, 158 (2004).
 - [12] C. Schäfermeier, M. Ježek, L. S. Madsen, T. Gehring, and U. L. Andersen, Deterministic phase measurements exhibiting super-sensitivity and super-resolution, *Optica* **5**, 60 (2018).
 - [13] T. Ono, R. Okamoto, and S. Takeuchi, An entanglement-enhanced microscope, *Nat. Commun.* **4**, 2426 (2013).
 - [14] A. N. Boto, P. Kok, D. S. Abrams, S. L. Braunstein, C. P. Williams, and J. P. Dowling, Quantum Interferometric Optical Lithography: Exploiting Entanglement to Beat the Diffraction Limit, *Phys. Rev. Lett.* **85**, 2733 (2000).
 - [15] R.-B. Jin and R. Shimizu, Extended Wiener–Khinchin theorem for quantum spectral analysis, *Optica* **5**, 93 (2018).
 - [16] N. Wiener, Generalized harmonic analysis, *Acta Math.* **55**, 117 (1930).
 - [17] A. Khintchine, Korrelationstheorie der stationären stochastischen prozesse, *Math. Annal.* **109**, 604 (1934).
 - [18] W. P. Grice and I. A. Walmsley, Spectral information and distinguishability in type-II down-conversion with a broadband pump, *Phys. Rev. A* **56**, 1627 (1997).
 - [19] D. Fröhlich, E. Mohler, and P. Wiesner, Observation of Exciton Polariton Dispersion in CuCl, *Phys. Rev. Lett.* **26**, 554 (1971).
 - [20] T. Itoh and T. Suzuki, Excitonic polariton-polariton resonance scattering via excitonic molecules in CuCl, *J. Phys. Soc. Jpn.* **45**, 1939 (1978).
 - [21] K. Edamatsu, G. Oohata, R. Shimizu, and T. Itoh, Generation of ultraviolet entangled photons in a semiconductor, *Nature (London)* **431**, 167 (2004).

- [22] H. Jayakumar, A. Predojević, T. Kauten, T. Huber, S. G. Solomon, and G. Weihs, Time-bin entangled photons from a quantum dot, *Nat. Commun.* **5**, 4251 (2014).
- [23] M. Ghali, K. Ohtani, Y. Ohno, and H. Ohno, Generation and control of polarization-entangled photons from GaAs island quantum dots by an electric field, *Nat. Commun.* **3**, 661 (2012).
- [24] Y. Chen, M. Zopf, R. Keil, F. Ding, and O. G. Schmidt, Highly-efficient extraction of entangled photons from quantum dots using a broadband optical antenna, *Nat. Commun.* **9**, 2994 (2018).
- [25] E. Schöll, L. Schweickert, L. Hanschke, K. D. Zeuner, F. Sbresny, T. Lettner, R. Trivedi, M. Reindl, S. F. C. da Silva, R. Trotta, J. J. Finley, J. Vučković, K. Müller, A. Rastelli, V. Zwiller, and K. D. Jöns, Crux of Using the Cascaded Emission of a Three-Level Quantum Ladder System to Generate Indistinguishable Photons, *Phys. Rev. Lett.* **125**, 233605 (2020).
- [26] P. G. Kwiat, K. Mattle, H. Weinfurter, A. Zeilinger, A. V. Sergienko, and Y. Shih, New High-Intensity Source of Polarization-Entangled Photon Pairs, *Phys. Rev. Lett.* **75**, 4337 (1995).
- [27] M. Gurioli, Z. Wang, A. Rastelli, T. Kuroda, and S. Sanguinetti, Droplet epitaxy of semiconductor nanostructures for quantum photonic devices, *Nat. Mater.* **18**, 799 (2019).
- [28] T. Mita, K. Sôtome, and M. Ueta, Stepwise two-photon excitation into excitonic molecule via exciton state of large wave vectors in CuCl, *J. Phys. Soc. Jpn.* **48**, 496 (1980).
- [29] E. Vanagas, J. Kudrna, D. Brinkmann, P. Gilliot, and B. Hönerlage, Phase relaxation dynamics of excitons and biexcitons in CuCl studied by femtosecond and picosecond degenerate four-wave mixing, *Phys. Rev. B* **63**, 153201 (2001).
- [30] H. Akiyama, T. Kuga, M. Matsuoka, and M. Kuwata-Gonokami, Radiative decay and phonon scattering of biexcitons in CuCl, *Phys. Rev. B* **42**, 5621 (1990).
- [31] T. Itoh, T. Katohno, and M. Ueta, Relaxation process of excitonic molecules in CuCl under the two-photon resonant excitation. I. Mutual collision of excitonic molecules, *J. Phys. Soc. Jpn.* **53**, 844 (1984).
- [32] H. Akiyama, M. Kuwata, T. Kuga, and M. Matsuoka, Biexciton lifetime in CuCl observed with weak picosecond pulse excitation, *Phys. Rev. B* **39**, 12973 (1989).
- [33] A. Dousse, J. Suffczyński, A. Beveratos, O. Krebs, A. Lemaître, I. Sagnes, J. Bloch, P. Voisin, and P. Senellart, Ultrabright source of entangled photon pairs, *Nature (London)* **466**, 217 (2010).
- [34] M. Rezai, J. Wrachtrup, and I. Gerhardt, Polarization-entangled photon pairs from a single molecule, *Optica* **6**, 34 (2019).
- [35] S. Shi, P. Kumar, and K. F. Lee, Generation of photonic entanglement in green fluorescent proteins, *Nat. Commun.* **8**, 1934 (2017).
- [36] R.-B. Jin, R. Shina, and R. Shimizu, Quantum manipulation of biphoton spectral distributions in a 2D frequency space toward arbitrary shaping of a biphoton wave packet, *Opt. Express* **26**, 21153 (2018).
- [37] Y. Mukai, R. Okamoto, and S. Takeuchi, Quantum Fourier-transform infrared spectroscopy in the fingerprint region, *Opt. Express* **30**, 22624 (2022).
- [38] J. Lavoie, T. Landes, A. Tamimi, B. J. Smith, A. H. Marcus, and M. G. Raymer, Phase-modulated interferometry, spectroscopy, and refractometry using entangled photon pairs, *Adv. Quantum Technol.* **3**, 1900114 (2020).